Coherent synchrotron emission in transmission from ultrathin relativistic laser plasmas

Coherent synchrotron emission in transmission from ultrathin relativistic laser plasmas

2013 New J. Phys. 15 015025

(http://iopscience.iop.org/1367-2630/15/1/015025)

New Journal of Physics
The open access journal for physics

Coherent synchrotron emission in transmission from ultrathin relativistic laser plasmas

B Dromey[1,5], S Cousens[1], S Rykovanov[2], M Yeung[1], D Jung[3,4], D C Gautier[4], T Dzelzainis[1], D Kiefer[2,3], S Palaniyppan[4], R Shah[4], J Schreiber[2,3], J C Fernandez[4], C L S Lewis[1], M Zepf[1] and B M Hegelich[3,4]

[1] Department of Physics and Astronomy, Centre for Plasma Physics, Queens University Belfast, Belfast BT7 1NN, UK
[2] Department für Physik, Ludwig-Maximilians-Universität, Am Coulombwall 1, D-85748 Garching, Germany
[3] Max-Planck-Institut für Quantenoptik, Hans-Kopfermann- Strasse 1, D-85748 Garching, Germany
[4] Los Alamos National Laboratory, Los Alamos, NM 87545, USA
E-mail: b.dromey@qub.ac.uk

New Journal of Physics **15** (2013) 015025 (14pp)
Received 21 August 2012
Published 31 January 2013
Online at http://www.njp.org/
doi:10.1088/1367-2630/15/1/015025

Abstract. Relativistic laser plasmas have been shown to provide a robust platform for the generation of bright attosecond pulses via the relativistically oscillating mirror and coherent wake emission mechanisms. Theoretical work, however, has shown an alternative method for achieving this goal: dense nanobunch formation and acceleration on timescales of less than an optical laser cycle ($\sim 10^{-15}$ s) during relativistic laser–plasma interactions. This opens up the exciting potential for developing a new bright ultrafast extreme ultraviolet XUV/x-ray source. Here we demonstrate, using a previously unexplored geometry, coherent synchrotron emission generated during relativistically intense laser–ultrathin foil interactions which extends to $\sim$1 keV photon energies. Particle-in-cell code simulations reveal how periodic sub-laser cycle acceleration of dense nanobunches of electrons formed during normal incidence interactions result in bursts of bright attosecond radiation in transmission and

[5] Author to whom any correspondence should be addressed.

how these pulses relate to plasma density scalelength. This work shows clear potential for a novel, intense source of attosecond XUV ($\sim 10^{-18}$ s) radiation. Experimentally, high order (n) harmonic spectra ($I(n)$) are characterized by a slow decay ($n^{-1.62}$) before a rapid efficiency rollover. Such a microscopic coherent synchrotron source ($< 5 \times 10^{-6}$ m) has the potential to significantly increase XUV pulse brightness significantly over current sources.

Contents

1. Introduction

The observation of bright, beamed extreme ultraviolet (XUV) harmonic radiation via the relativistically oscillating mirror (ROM) [1–7] and the coherent wake emission (CWE) [8–11] mechanisms have show that relativistic laser–plasma interactions can be tailored experimentally to support coherent XUV pulse generation. Recent theoretical work, however, has revealed that under certain conditions the potential also exists for generating harmonic radiation via coherent synchrotron emission (CSE) during the interaction of intense lasers with steep density gradient plasma–vacuum boundaries, dramatically boosting the generated harmonic efficiency [7, 12]. Experimentally it has been shown that characteristic CSE spectra can be generated during normal incidence interactions in the transmitted direction [13]. Here we discuss the principle of CSE and the fundamental physics relating to its generation during relativistic laser–plasma interactions.

Synchrotron radiation from insertion devices in large electron storage rings (>10 m diameter) has been at the forefront of XUV/x-ray science for many decades. In principle, the instantaneous brightness of these machines can be increased substantially by the formation of dense nanobunches of electrons to permit CSE. XUV and x-ray radiation ($\lambda < 100$ nm) produced by synchrotron emission is typically temporally incoherent due to the longitudinal electron bunch length, δ, being many times the coherence length, $l_c < \frac{\lambda}{2}$, for emission at λ. The instantaneous radiation intensity spectrum for such an N particle bunch is given by

$$\frac{\mathrm{d}I}{\mathrm{d}\omega_N} = \frac{\mathrm{d}I}{\mathrm{d}\omega_1}[N + N(N-1)\tilde{f}(\omega)], \tag{1}$$

where $\mathrm{d}I/\mathrm{d}\omega_1$ is the far field emitted intensity per spectral bandwidth of a single particle and $\tilde{f}(\omega)$ is the Fourier transform of the normalized longitudinal electron density distribution [14]. Assuming a Gaussian density profile, for $\delta \gg l_c$, $\tilde{f}(\omega)$ is essentially 0 and (1) is a linear sum over N, or incoherent synchrotron emission. If, on the other hand, $\delta \leqslant l_c$, $\tilde{f}(\omega)$ becomes non-zero and the $\sim N^2$ term dominates i.e. emission from the entire bunch can constructively

interfere (coherent superposition) and very bright attosecond pulse formation is possible due to the short l_c of the emission.

Producing electron bunches of sufficiently small spatial dimension to extend the principle of CSE to the x-ray regime is currently beyond what is considered achievable with conventional large scale accelerators. Simulations investigating the dynamics of relativistic laser–plasma interactions have, however, shown that it is in principle possible for dense electron nanobunches (i.e. 10^{-9} m scale) to be formed on ultrafast timescales ($< 10^{-15}$ s) both in the reflected [15] and transmitted [16] directions. Going one step further, recent work has shown that under certain conditions bunches formed and accelerated by the strong fields of a relativistically intense laser pulse can permit the generation of CSE extending to the x-ray regime in specular reflection during p-polarized, oblique incidence laser–solid target interactions [7, 12].

For many cycle laser pulses, the experimental signature of this process is the emission of high-order harmonics. Other sources of high harmonic spectra, such as the CWE and ROM mechanisms, summarized here as surface high harmonic generation (SHHG) processes, will in general compete with CSE in reflection especially given the slightly more relaxed constraints on plasma density scalelength required for efficient generation [7]. For this reason experiments studying harmonic generation have not observed CSE as a dominant generation mechanism to date. As a result we focus our discussion here on identifying and demonstrating experimentally a novel method to observe laser-driven CSE extending to the x-ray spectral region—relativistically intense laser interactions from ultrathin foils from a '*normal incidence in transmission*' geometry.

2. Isolation and generation of coherent synchrotron emission (CSE) with respect to other surface high harmonic generation mechanisms

As mentioned above the experimentally observed signature of periodic, sub-laser cycle emission of coherent XUV/x-ray pulses is high harmonic generation (HHG) and can equivalently be called 'attosecond interference'. In the limit of single XUV pulse emission, no interference can occur and a continuous spectrum is observed i.e. no harmonics.

Driven by relativistically intense laser pulses ($>10^{18}$ W cm^{-2}) at the surface of a solid density target, SHHG occurs due to electrons performing complex trajectories determined by multiple laser absorption mechanisms [6, 17]. In this sense SHHG is an umbrella term covering multiple, distinct harmonic generation processes. To date, harmonic spectra extending to high orders (>20) observed experimentally in specular reflection from solid targets are consistent with ROM scaling. In this scheme the critical density plasma surface (i.e. a highly reflective mirror-like surface with respect to the incident laser radiation) is driven in the strong laser field and as a result the reflected light contains frequency up-shifted components theoretically described as an oscillatory extension to Einstein's relativistic flying mirror. Referred to as the theory of relativistic spikes, this mechanism implies a $n^{-8/3}$ power-law decay [2] in the harmonic spectrum being dominant.

This $n^{-8/3}$ scaling is applicable for harmonic orders n above the CWE cutoff order, n_{CWE} [8], which is the harmonic order corresponding to the maximum plasma frequency ω_{pmax} of the target. This can be calculated as

$$n_{\mathrm{CWE}} = n_{\omega\mathrm{max}} = \omega_{\mathrm{pmax}}/\omega_{\mathrm{L}} = \sqrt{N_{\mathrm{emax}}/N_{\mathrm{c}}}, \tag{2}$$

where ω_L is the laser frequency, N_{emax} is the peak electron density of the target and $N_c = \frac{\epsilon_0 m_e \omega_L^2}{e^2}$ is called the critical density, which depends on the electron charge e and mass m_e. For efficient CWE generation in reflection a p-polarized, oblique (45°) incidence interaction is required [8]. Here we discuss harmonic generation in the spectral region $n > n_{CWE}$ to avoid any possible ambiguity with this mechanism.

As mentioned above, recent theoretical work has shown how CSE can be generated into the specularly reflected direction during p-polarized, oblique incidence interactions [7, 12]. This process relies on the formation of dense nanobunches of electrons at the vacuum–solid interface during oblique incidence relativistically intense interactions. An der Brugge and Pukhov [7, 12] identify conditions under which such bunches can emit CSE for few (<5) cycle interactions. CSE is characterized by a nearly flat, synchrotron-like spectrum ($I(n) \sim n^{-4/3}$ to $n^{-6/5}$) up to a rollover frequency ω_{rs} that is intrinsically linked to δ and the maximum Lorentz factor $\gamma_{max} = (\sqrt{1-(v/c)^2})^{-1}$ of the nanobunch. Above ω_{rs} the spectrum exhibits a rapid exponential rollover [12].

While it is clear that there are several mechanisms for SHHG in reflection, examining the problem from a flipped geometry presents an interesting proposition—is it possible to observe harmonic radiation in the transmitted direction during normal incidence interactions with ultrathin relativistic laser plasmas (i.e. significantly thinner that the driving laser wavelength) and what is the origin of such radiation?

The fundamental generation mechanism for ROM harmonic generation is the relativistic Doppler effect [18], or to be more precise, an oscillatory extension to it. However, the basic physics of Doppler up-shifting still holds and can be easily understood when considering an electron in constant motion with a Lorentz factor of γ towards a source with frequency ω. The electron experiences radiation in its rest frame up-shifted by factor of 2γ. Radiation reemitted towards the observer is then also up-shifted by a factor 2γ and is subsequently detected in the lab frame at a frequency of $4\gamma^2\omega$. On the other hand radiation emitted in the forward direction is downshifted by a factor of 2γ and hence is detected at the initial frequency ω. Therefore the ROM mechanism [1–7] is completely cancelled for a transmitted geometry. Take the simple example of a 50 : 50 partial reflector travelling with relativistic velocities for $4\gamma^2$ up-shifting of a counterpropagating light pulse: in this scenario the transformation that results in up-shifting for reflection, (which implies a change in the sign of the k-vector of the light), is completely cancelled in the transmitted direction (i.e. no change in the sign of the k-vector). If this example is extended to one of a partial reflector oscillating about a rest point, it is clear that when the transmitted light and the mirror are moving in the same direction no up-shift is possible.

On the other hand, for CSE to be possible it is clear that dense nanobunches of electrons must be formed during relativistic laser–plasma interactions. Taking the very simple example of a laser incident in normal incidence on an ultrathin foil (thickness $< \lambda_{laser}$) we study nanobunch formation in the transmitted direction in figures 1 and 2 using the PICWIG one-dimensional(1D) particle in cell code [19].

In figure 1 the electron density is saturated at $20N_c$, where N_c is the critical density for the laser fundamental wavelength. As can be seen the electron nanobunches produced during this specific interaction have densities on the order of $10N_c$ at the time of emission through the rear surface of the target. Furthermore, as can be seen in figure 2, the nanobunches have a spatial extent of $<0.01\lambda_L$, the driving laser wavelength, implying that such bunches will readily fulfil the criteria for CSE generation right down to sub 10 nm for $\lambda_L = 1\ \mu$m.

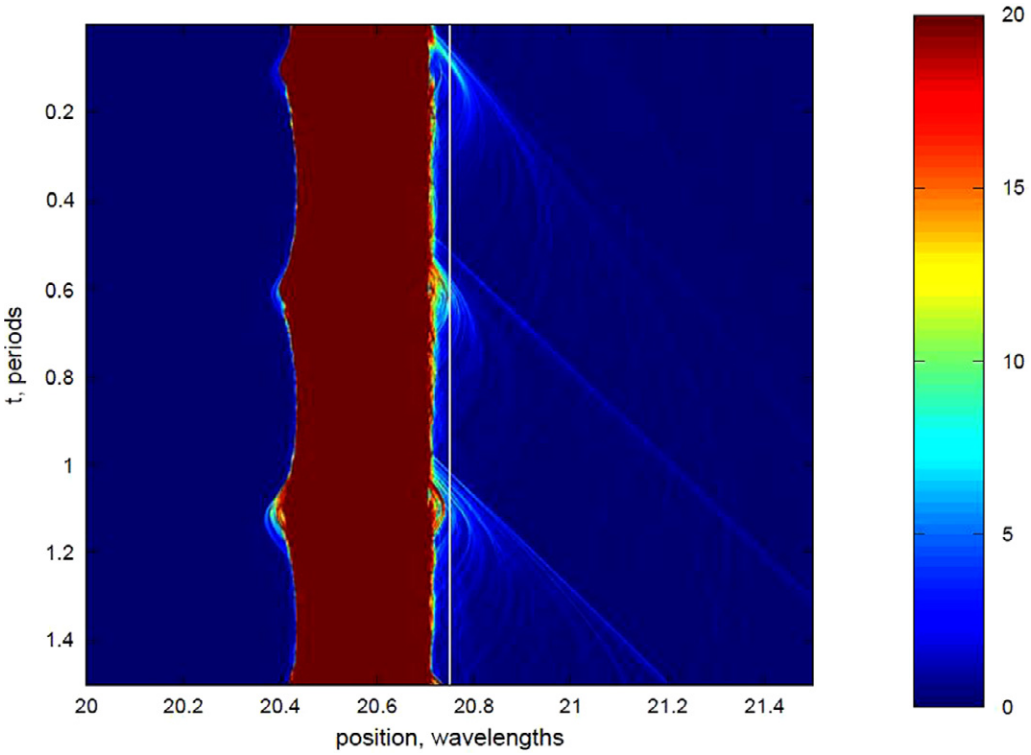

Figure 1. Dense electron nanobunch formation studied using the PICWIG 1D particle in cell code [19] for 200 nm thick foil and 100 nm linear ramp to vacuum, 10 cycle pulse, normalized vector potential $a_0 = 10$, where $a_0 = \sqrt{I_L \lambda_L^2/(1.37 \times 10^{18}\,\mathrm{W}\,\mu\mathrm{m}^2\,\mathrm{cm}^{-2})}$, and I_L and λ_L are the focused intensity and wavelength of the driving laser (1 μm), max density $= 80N_c$. The density is saturated at $20N_c$. Colour scale is in units of N_c.

3. CSE in transmission from ultrathin relativistic plasmas

To investigate the emission of coherent XUV radiation in the transmitted direction we first study the interaction of a relativistically intense laser pulse normally incident onto an ultrathin foil (thickness $< \lambda_{laser}$) using the PICWIG 1D particle in cell code [19]. Here we choose a few cycle laser pulse to demonstrate the generic formation of electron nanobunches during such interactions and how these nanobunches directly lead to CSE in the transmitted direction.

Studying the formation and motion of such nanobunches it becomes clear that as the bunches reach maximum density they perform very rapid circular/elliptical trajectories at the front surface of a sharp plasma vacuum interface target before being driven in the transmitted direction and emitted through the rear surface of the target (figure 3). This rapid acceleration leads to the emission of attosecond bursts of XUV radiation in transmission (figure 4).

These sharp well defined, periodic bursts of attosecond bursts of XUV radiation in transmission via the CSE mechanism leads to strong, well defined harmonic emission in the spectral domain (figure 5).

This temporally localized, periodic emission only occurs under the conditions where dense nanobunches of electrons can form at the front surface of a target with ultrashort/step plasma

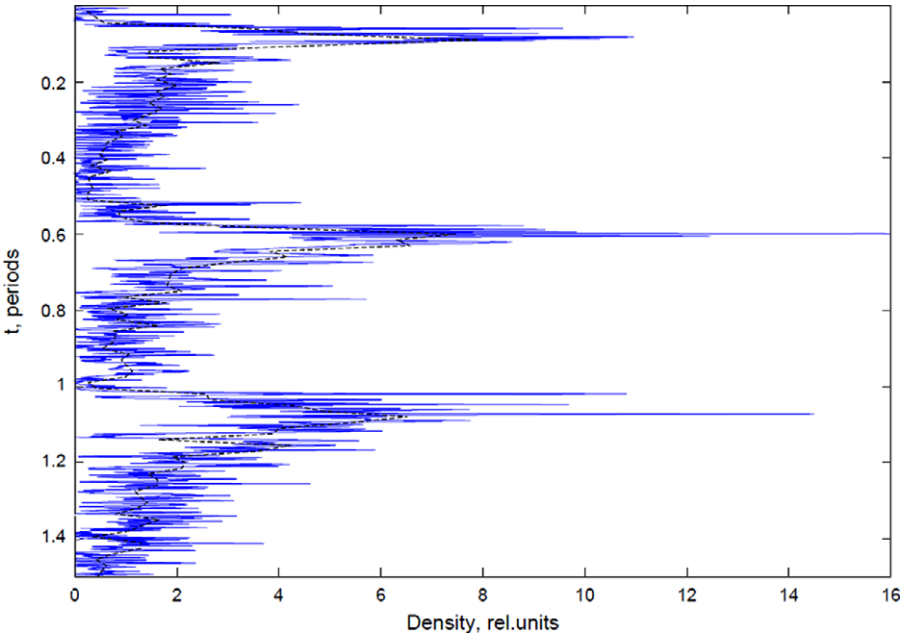

Figure 2. Dense electron nanobunch formation studied using the PICWIG 1D particle in cell code [19] for 200 nm thick and 100 nm linear ramp to vacuum, 10 cycle pulse, $a_0 = 10$, max density $= 80N_c$, driving wavelength 1 μm. The figure shows the density profile along the white line at the rear of the target in figure 1.

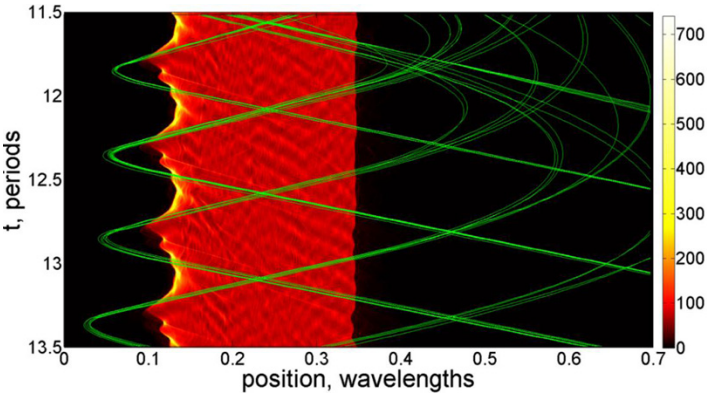

Figure 3. Dense nanobunch formation during normal incidence interaction studied using the PICWIG 1D particle in cell code [19]. Simulation parameters: 200 nm thick, max density $= 80N_c$, step like density profile from 0 to $80N_c$, 10 cycle full width half max pulse, $a_0 = 10$. Simulations were performed with 1000 cells per wavelength and 400 particles per cell. Here trajectories of those quasi-electrons that gained longitudinal momentum $p_x > 5$ during two laser cycles are shown to highlight the bunching and trajectories performed at the front surface.

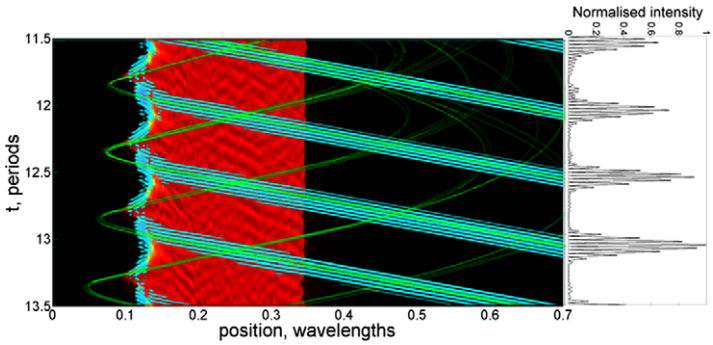

Figure 4. The emitted XUV intensity in the transmitted direction as a function of time during the normal incidence interaction described in figure 3. Here XUV emission (18–25th harmonic) during two laser cycles in the transmitted direction is shown, demonstrating the origin of the emission is from the trajectories of dense nanobunches at the front surface of the target.

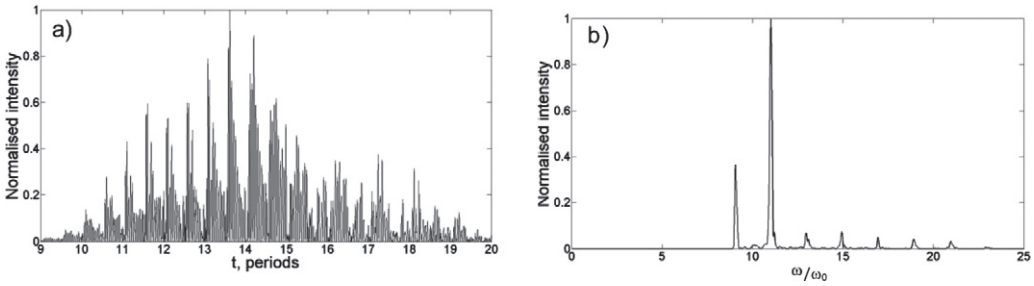

Figure 5. Attosecond pulse structure and corresponding harmonic spectrum for the interaction described in figures 3 and 4. Note the suppression of harmonic orders below 8 due to plasma opacity, confirming emission from the front surface.

density scalelengths. Increasing the plasma density ramp length towards significant fractions of the driving laser wavelength inhibits well defined bunch formation and subsequently attosecond localization of XUV emission. This can clearly be observed in figures 6 and 7 where the scalelength is increased to 800 nm from 0 to $80N_c$. Another key feature of these bunches is that the number of contributing trajectories is significantly reduced, implying significantly reduced bunch density.

As can be seen in figure 7 the sharp well defined, periodic bursts of attosecond bursts of XUV radiation in transmission via the CSE mechanism are inhibited by the extended plasma scalelength i.e. instead of four well defined bursts there are now only two extended regions of emission (figure 7). This destruction of well localized XUV bursts leads to significant breakup in harmonic structure in the emitted spectrum (figure 8).

How this resulting aperiodicity relates to the overall generation mechanism and experimentally observed beam characteristics will be the subject of a future publication. It is important to note that since these are 1D simulations all of the radiation in transmission is analysed in the spectra presented in figures 5 and 8. However, it is clear from preliminary two-dimensional (2D) simulations and experiments performed on the Trident laser system (beyond the scope of this discussion) that the increased plasma scale length leads to significant CSE

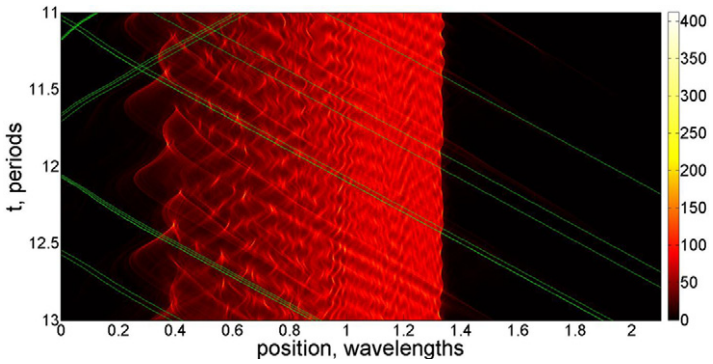

Figure 6. Inhibited periodicity of nanobunch formation during normal incidence interaction due to increased plasma scalelength studied using the PICWIG 1D particle in cell code [19]. Simulation parameters: 200 nm thick target with 800 nm density ramp from front surface, 10 cycle full width half max pulse, $a_0 = 10$, max density $= 80N_c$. Simulations were performed with 1000 cells per wavelength and 400 particles per cell. Here trajectories of those quasi-electrons that gained longitudinal momentum $p_x > 5$ during two laser cycles are shown to highlight the bunching and trajectories performed at the front surface.

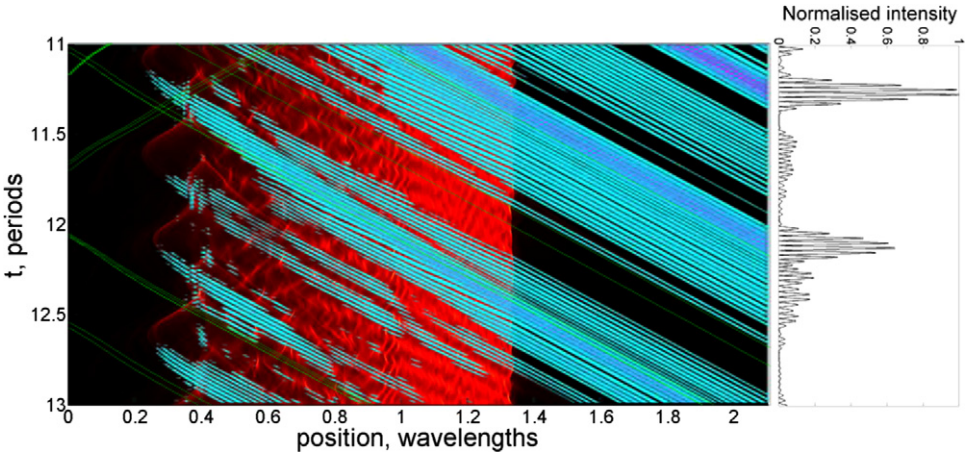

Figure 7. The emitted XUV intensity in the transmitted direction as a function of time during the normal incidence interaction described in figure 6. Here XUV emission (19–25th harmonic inclusive) during two laser cycles in the transmitted direction is shown, demonstrating the destruction of attosecond structure in the emission.

beam scattering into wide angles along with a destruction of overall harmonic structure in the emitted radiation.

4. Experimental observation of CSE in transmission

To examine the generation of CSE experimentally we performed experiments at both the Trident (500 fs, ~80 J, focused intensity $\sim 4 \times 10^{20}$ W cm^{-2}) [13, 20] and Astra Gemini (50 fs, ~10 J,

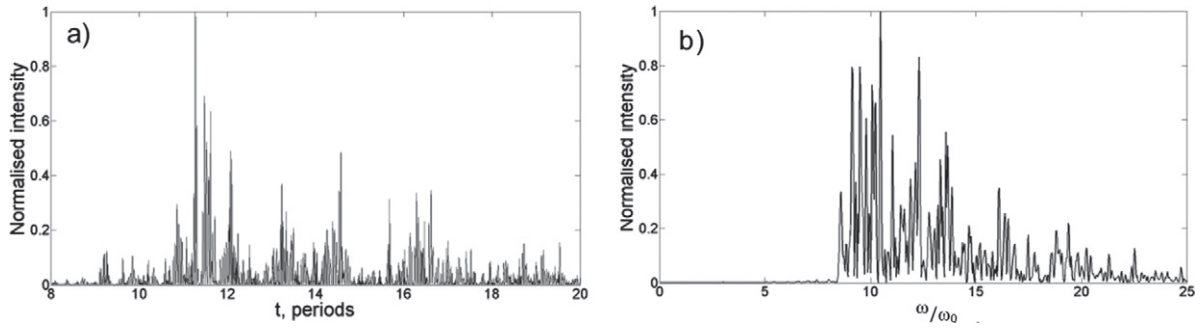

Figure 8. XUV pulse structure (a) and corresponding harmonic spectrum (b) for the interaction described in figures 6 and 7.

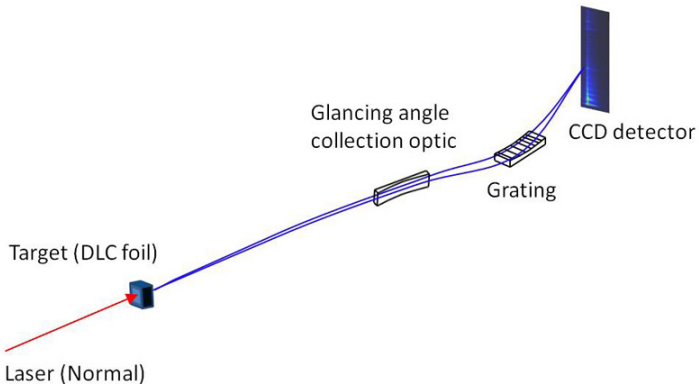

Figure 9. Schematic of experimental setup to observe CSE on the Trident laser at Los Alamos [13]. XUV spectral content was analysed using a grazing incidence Hitachi flatfield grating and the radiation was detected using a back thinned Andor XUV CCD.

focused intensity $\sim 10^{20}\,\mathrm{W\,cm^{-2}}$) laser systems. In both experiments XUV radiation is studied in transmission through 200 nm diamond-like-carbon (DLC) and carbon foils during normal incidence interactions. A typical schematic of the experimental arrangement is shown figure 9.

The Trident Laser Facility at Los Alamos National Laboratory is a Nd:glass ($\lambda_L = 1053$ nm) system delivering laser pulses with an energy of $E_L = 80$ J in 500 fs focused to a near diffraction limited focal spot using an $F/3$ off-axis parabolic mirror. With this system a laser peak to prepulse level contrast of $1{:}10^{-10}$ at $\sim$1 ns (10^{-9} s) and $1{:}10^{-7}$ at $\sim$10 ps(10×10^{-12} s) is achieved. The 'near-time' (sub 10 ps) shot-to-shot variation in pulse contrast was measured using a single shot third order autocorrelator, showing typical values of $\sim 1 : 10^{-4}$ at 2 ps. It should be noted that contrast enhancing plasma mirrors typical of relativistic laser plasma based harmonic generation were not required. Figure 10 shows spectra obtained in transmission from Trident using 200 nm DLC foils. These are characterized by a shallow decay to higher orders with a rapid rollover for harmonic orders >70.

In figure 11 the spectra are deconvolved to reveal the relative efficiency scaling with respect to harmonic order. In addition to the spectra presented in figure 10, which primarily show on laser axis harmonic emission collected from a $\sim 3^\circ$ cone, spectra were also collected from wider angles (up to $\pm 8.2^\circ$) to ensure full harmonic beam collection for accurate efficiency estimation.

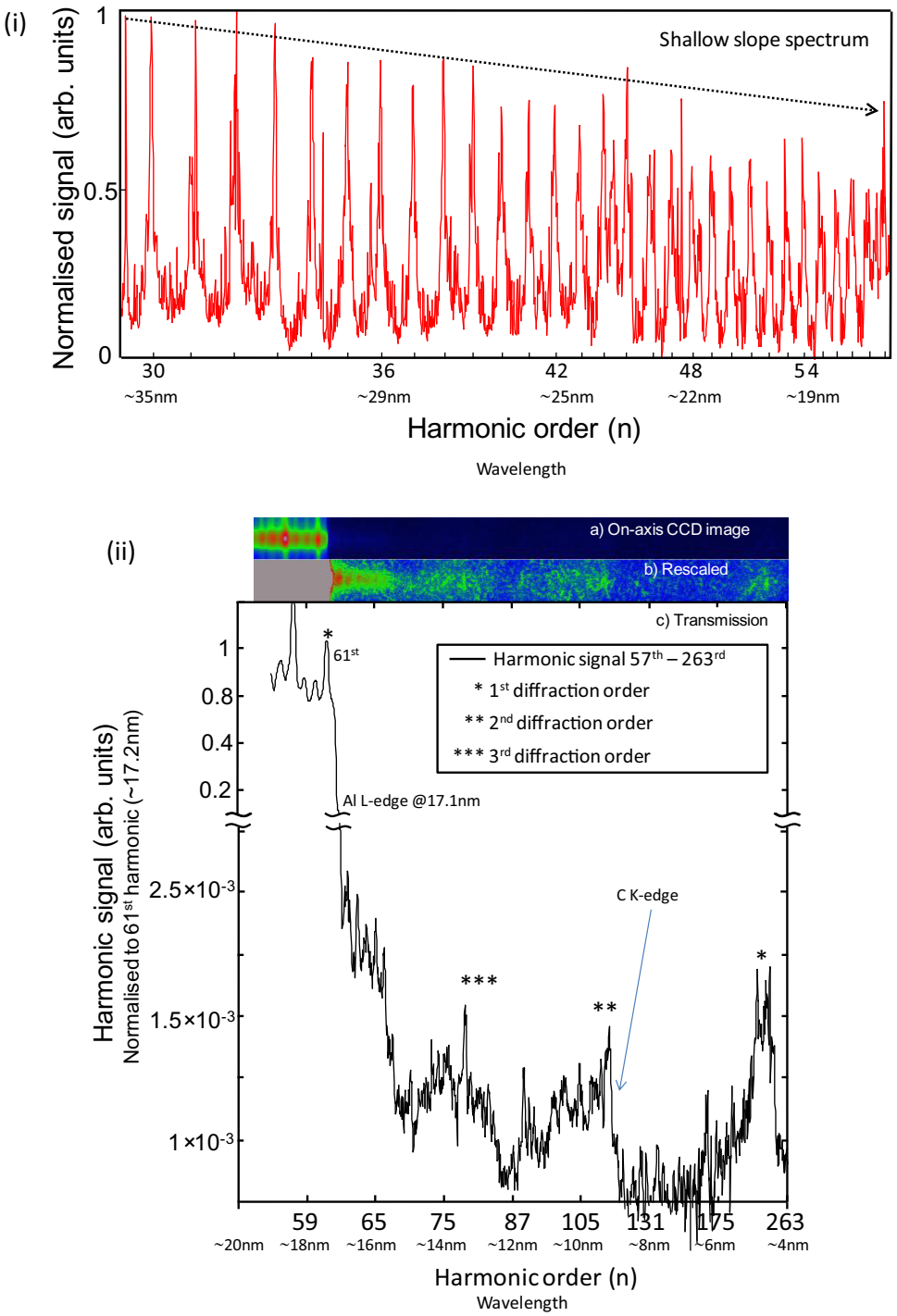

Figure 10. Harmonic spectra generated in transmission from 200 nm DLC foils on the Trident laser. Figure (i) shows harmonic emission in the spectral region 35–17 nm and (ii) shows emission in the region 20–4 nm. Multiple diffraction orders (1–3) are visible in (ii) due to the transmission function of the spectrometer which uses a 0.2 μm Al filter to block optical radiation. The spectrum is normalized at the 61st harmonic order (labelled 61st). Figure (ii)

Figure 10. (Continued) (a) and (b) are the raw CCD images of the spectrum, scaled to show both high and low orders. (c) is the corresponding spectrum from integration in the spatial (vertical) direction. It is worth noting that while only odd orders are observed in 1D simulations (figure 5) we observe both odd and even orders in the experiment. Preliminary 2D simulations indicate that is due to the angular distribution of the signal resulting in additional interferences in the observed spectrum. This detailed discussion will be the subject of a future publication.

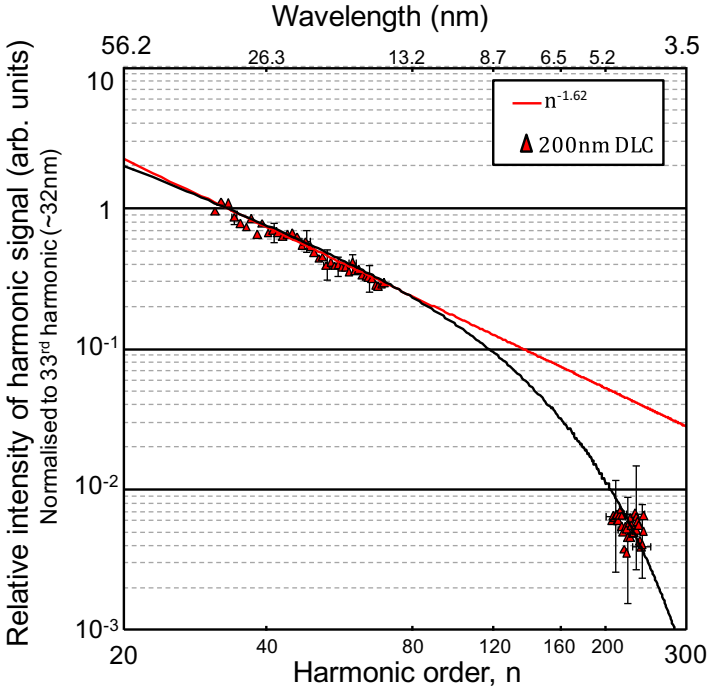

Figure 11. Deconvolved spectrum showing shallow scaling of harmonic orders extending to $\sim n = 70$ before a rapid rollover in spectral efficiency to high orders. Spectral deconvolution is obtained by analysis of harmonic emission generated in transmission on and off the laser axis and accounting for spectrometer transmission. The red line is an $n^{-1.62}$ fit to the harmonic signal for orders <70. The black solid line is a guide to the shape of the real spectrum. The bars represent the uncertainty in the signal after deconvolution [13].

Additional experiments analysing both on and off axis XUV radiation confirm beam cone narrowing with harmonic order, indicating a high degree of spatial coherence at the generation point. See [13] for a full discussion on spectral deconvolution and scaling.

For orders below $\sim n = 70$ the scaling of the harmonic signal from 200 nm DLC targets decays as $n^{-(1.62,+0.12,-0.13)}$. This is approaching the $I(n) \sim n^{-4/3}$ to $n^{-6/5}$ scaling suggested for the CSE mechanism in reflection, and is significantly higher than the $n^{-8/3}$ scaling predicted for the ROM mechanism in reflection. This observation represents a significant step forward in the generation of bright XUV/x-ray sources with attosecond potential, in particular since, for the

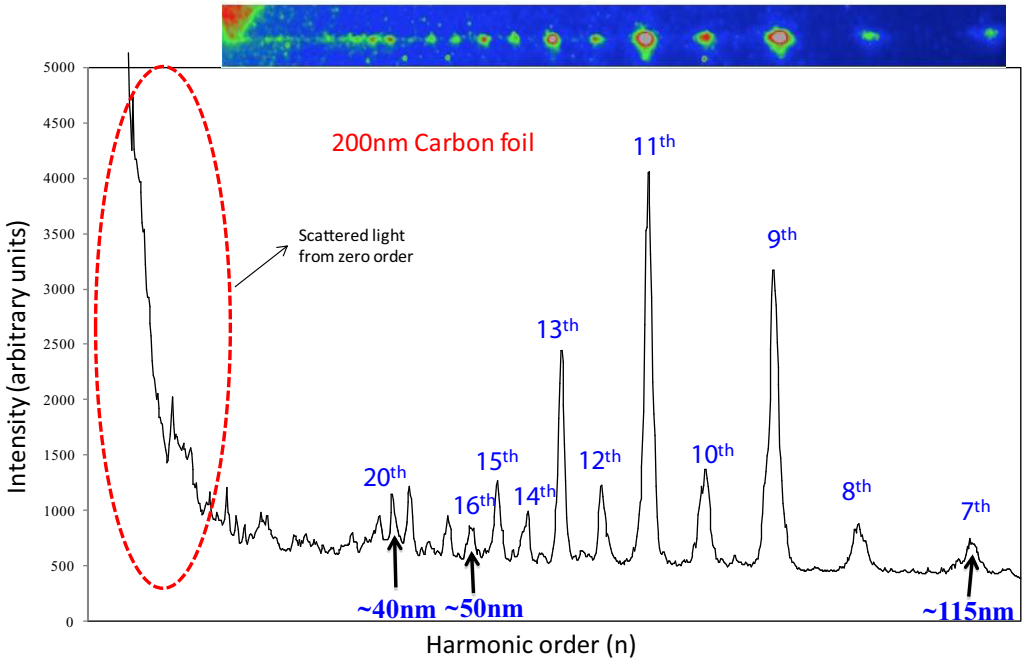

Figure 12. Harmonic spectrum generated in transmission from 200 nm carbon foils on the Astra Gemini laser system.

first time, harmonic emission extending far above the CWE cut-off n_{CWE} has been observed in a geometry where ROM cannot exist. Moreover, the observation of spectra with scaling approaching the characteristic scaling of CSE offers clear evidence of dense electron nanobunch driven XUV emission [13].

We have also performed similar experiments using the 50 fs Astra Gemini laser. The Astra Gemini laser at Rutherford Appleton Laboratories is a Titanium Sapphire ($\lambda_{\mathrm{L}} = 800$ nm) system delivering laser pulses with an energy of $E_{\mathrm{L}} = 10$ J in 50 fs focused to a near diffraction limited focal spot using an $F/2$ off-axis parabolic mirror. With this system a laser peak to prepulse level contrast of $1{:}10^{-10}$ at $\sim$10 ps(10^{-11} s) and $1{:}10^{-9}$ at $\sim$2 ps(10×10^{-12} s) is achieved using a contrast enhancing double plasma mirror setup. Closer in time to the pulse is a rapid rise to peak intensity.

Spectra in transmission are obtained using 200 nm carbon foils and are characterized by a sudden increase in the observed signal at the ninth harmonic followed by a peaked spectrum which decays slowly to high orders (see figure 12). Again this spectral shape is not characteristic of a monotonically decaying harmonic generation mechanism such as those observed in reflection (CWE and ROM) and while more work is required to understand the complete nature of the differences between long (500 fs) and short (50 fs) interactions the observation of such spectra is already strong evidence for the novel CSE mechanism to be the dominant process governing this emission.

It should be noted that previous studies of HHG in transmission have been almost exclusively performed in oblique incidence [15–17]. Under these circumstances it is possible to observe CWE in transmission. For CWE, relativistic currents at the rear of the target can produce density waves which can undergo linear mode conversion [15, 17]. Oblique incidence

experiments examining harmonic emission above ω_{pmax} in the transmitted direction were at significantly lower contrast to that presented here. The inherent contrast of laser pulses used in the experiment reported by Krushelnick *et al* [21] was 10^{-6} on the ns scale, and 10^{-4} at 50 ps, which is sufficient to support large scale plasma instability formation leading to very wide angle scatter of ROM from the front surface. This is fundamentally different to the significantly higher contrast interaction reported in our manuscript which supports harmonic beaming, wavelength/harmonic dependent cone narrowing [13] and very slow spectral decay to higher energies before a rapid efficiency rollover, all consistent with predictions for CSE.

5. Outlook and conclusion

In conclusion, we present a novel geometry under which it is possible to isolate and observe CSE for the first time experimentally. Simulations reveal how dense nanobunch formation during normal incidence, short plasma density scalelength interactions permit the generation of attosecond bursts of XUV radiation in the transmitted direction and, by extension, harmonic spectra in the transmitted direction with shallow scaling characteristic of CSE.

Future experiments will focus on optimizing the absolute generation efficiency by examining target materials and thicknesses, and importantly the role plasma scalelength plays in the production of periodic attosecond pulses and overall beam characteristics of the emitted radiation.

References

[1] Bulanov S V, Naumova N M and Pegoraro F 1994 Interaction of an ultrashort, relativistically intense laser-pulse with an overdense plasma *Phys. Plasmas* **1** 745–57
[2] Baeva T, Gordienko S and Pukhov A 2006 Theory of high-order harmonic generation in relativistic laser interaction with overdense plasma *Phys. Rev.* E **74** 046404
[3] Gibbon P 1996 Harmonic generation by femtosecond laser–solid interaction: a coherent 'water-window' light source? *Phys. Rev. Lett.* **76** 50–3
[4] Dromey B *et al* 2006 Harmonic generation in the relativistic limit *Nature Phys.* **2** 456
[5] Dromey B *et al* 2007 Bright multi-keV harmonic generation from relativistically oscillating plasma surfaces *Phys. Rev. Lett.* **99** 085001
[6] Teubner U and Gibbon P 2009 High-order harmonics from laser-irradiated plasma surfaces *Rev. Mod. Phys.* **81** 445
[7] An der Brugge D and Pukhov A 2011 Theory of attosecond pulses from relativistic surface arXiv:1111.4133v1
[8] Quéré F, Thaury C, Monot P, Dobosz S, Martin Ph, Geindre J-P and Audebert P 2006 Coherent wake emission of high-order harmonics from overdense plasmas *Phys. Rev. Lett.* **96** 125004
[9] Carman R L, Forslund D W and Kindel J M 1981 Visible harmonics emission as a way of measuring profile steepening *Phys. Rev. Lett.* **46** 29
[10] Teubner U *et al* 2004 Harmonic emission from the rear side of thin overdense foils irradiated with intense ultrashort laser pulses *Phys. Rev. Lett.* **92** 185001
[11] Brunel F 1987 Not-so-resonant, resonant absorption *Phys. Rev. Lett.* **59** 52–5
[12] Pukhov A, An der Brugge D and Kostyukov I 2010 Relativistic laser plasmas for electron acceleration and short wavelength radiation generation *Plasma Phys. Control. Fusion* **52** 124039
[13] Dromey B *et al* 2012 Coherent synchrotron emission from electron nanobunches formed in relativistic laser–plasma interactions *Nature Phys.* **8** 804–8

[14] Schiff L I 1946 Production of particle energies beyond 200 MeV *Rev. Sci. Instrum.* **17** 6
[15] Naumova N M, Nees J A, Sokolov I V, Hou B and Mourou G A 2004 Relativistic generation of isolated attosecond pulses in a λ^3 focal volume *Phys. Rev. Lett.* **93** 195003
[16] Popov K I *et al* 2006 Vacuum electron acceleration by tightly focused laser pulses with nanoscale targets *Phys. Plasmas* **16** 053106
[17] Wilks S C *et al* 1992 Absorption of ultra intense light pulses *Phys. Rev. Lett.* **69** 1383
[18] Einstein A 1905 On the electrodynamics of moving bodies *Ann. Phys., Lpz.* **17** 891
[19] Rykovanov S G, Geissler M, Meyer-ter-Vehn J and Tsakiris G D 2008 Intense single attosecond pulses from surface harmonics using the polarization gating technique *New J. Phys.* **10** 025025
[20] Batha S *et al* 2008 TRIDENT high-energy-density facility experimental capabilities and diagnostics. *Rev. Sci. Instrum.* **79** 10F305
[21] Krushelnick K *et al* 2008 Effect of relativistic plasma on extreme-ultraviolet harmonic emission from intense laser–matter interactions *Phys. Rev. Lett.* **100** 125005